1-1-2007

Formation, thermal stability, and surface composition of size-selected AuFe nanoparticles

A. Naitabdi
University of Central Florida

Roldan Cuenya
University of Central Florida

Formation, thermal stability, and surface composition of size-selected AuFe nanoparticles

Cite as: Appl. Phys. Lett. **91**, 113110 (2007); https://doi.org/10.1063/1.2784957
Submitted: 18 July 2007 . Accepted: 23 August 2007 . Published Online: 13 September 2007

A. Naitabdi, and B. Roldan Cuenya

Formation, thermal stability, and surface composition of size-selected AuFe nanoparticles

A. Naitabdi and B. Roldan Cuenya[a)]
Department of Physics, University of Central Florida, Orlando, Florida 32816, USA

(Received 18 July 2007; accepted 23 August 2007; published online 13 September 2007)

The surface composition of isolated $Au_{0.5}Fe_{0.5}$ nanoparticles (NPs) synthesized by micelle encapsulation and supported on $TiO_2(110)$ has been investigated. The study reveals that phase-segregated structures are present after annealing at 300 °C. A subsequent thermal treatment at 700 °C resulted in the formation of a AuFe alloy. At this temperature, a state characteristic of Fe was identified at the NPs' surface. Annealing at 900 °C resulted in the disappearance of the Fe surface state, which is attributed to Au segregation to the surface. The initial hexagonal NP arrangement on the $TiO_2(110)$ surface was preserved up to 900 °C. At 1000 °C, Au desorption was observed. © *2007 American Institute of Physics*. [DOI: 10.1063/1.2784957]

The physical and chemical properties of bimetallic alloy nanostructures differ strongly from those of their monometallic counterparts.[1–4] In the field of heterogeneous catalysis, oxide-supported bimetallic nanoparticles are known to exhibit remarkably high activities and enhanced selectivities. This is due to their ability to lower the energy barrier of a specific chemical reaction[5] and their enhanced resistance against poisoning.[6] AuFe clusters have been proven active for the structure-sensitive low-temperature CO oxidation[7] reaction. However, the structure and thermal stability of AuFe nanoparticles (NPs) are still not well understood.

In the present work, scanning tunneling microscopy and spectroscopy (STM and STS) were used to investigate the surface composition of self-assembled size-selected AuFe nanoparticles. Differential conductivity (dI/dV) spectra were measured on the surface of isolated AuFe NPs after different annealing treatments to gain insight into their local density of states (LDOS). This local spectroscopic method has been used in the past to identify the chemical composition of surface alloys containing Fe: Fe/Pt(111),[8] Cr/Fe(001),[9] and Au/Fe(001).[10] The well-known Fe surface state near the Fermi level (E_F) (Ref. 11) which appears as a sharp feature in the dI/dV curves is used as a signature of the presence of Fe atoms at the NP surface.

Self-assembled size-selected $Au_{0.5}Fe_{0.5}$ NPs were synthesized by encapsulation in diblock-copolymer micelles formed by dissolving polystyrene-block-poly(2-vinylpyridine) [PS(x)-P2VP(y), with molecular weights $x=81000$ and $y=14200$ g/mol] in toluene. Subsequently, two metal salts, ($HAuCl_4 \cdot 3H_2O$) and ($FeCl_3$) were added simultaneously at equal concentration to the polymeric solution. The complete encapsulation of the Au and Fe compounds inside the micelles was achieved when a metal salt to PS-P2VP concentration ratio of 0.6 was used. Following this synthesis method, for a given particle size [determined by the molecular weight of the polymer core (P2VP)], the alloy composition can be easily tuned by changing the relative concentration of the two metal salts. The interparticle distance is determined by the length of the polymer tail (PS). A monolayer-thick film of NPs was obtained by dip coating (*ex situ*) a $TiO_2(110)$ single crystal into the gold-iron polymeric solution. This substrate was previously cleaned in ultrahigh vacuum (UHV) by Ar^+ sputtering (1 keV) and annealing cycles at 950 °C to obtain optimum conductive properties.[12] The sample was then introduced into a UHV system (SPECS, GmbH) for *in situ* chemical and electronic characterizations. The encapsulating polymer was removed *in situ* by O_2-plasma exposure (4.5×10^{-5} mbar, 80 min). Complete removal of the organic ligands was evidenced by the lack of C 1*s* signal in x-ray photoelectron spectroscopy (XPS) measurements. Subsequently, the sample was annealed *in situ* for 20 min at 100 °C intervals from 300 to 800 °C and at 900 and 1000 °C for 10 min. XPS and STM data were acquired after each thermal treatment. In order to minimize scanning artifacts due to tip contamination, our chemically etched W tip was cleaned by Ar^+ sputtering (4 keV, 4.3 μA) prior to each STS session.

Figure 1 shows STM images acquired at 15 °C on AuFe

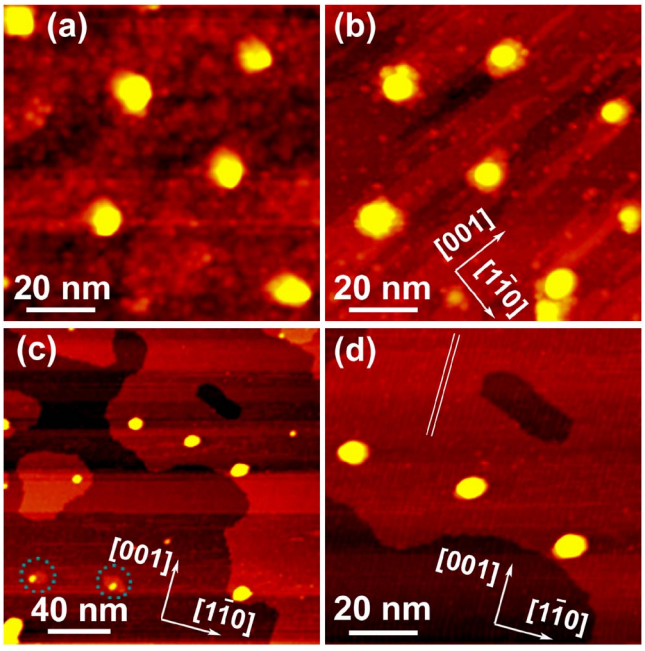

FIG. 1. (Color online) STM images ($V_t=1.0$ V, $I_t=0.30$ nA) of $Au_{0.5}Fe_{0.5}$ NPs on $TiO_2(110)$ measured at 15 °C after an O_2-plasma treatment and subsequent annealing at 300 °C (20 min) (a), 900 °C (10 min) (b), and 1000 °C (10 min) [(c) and (d)].

[a)]Electronic mail: roldan@physics.ucf.edu

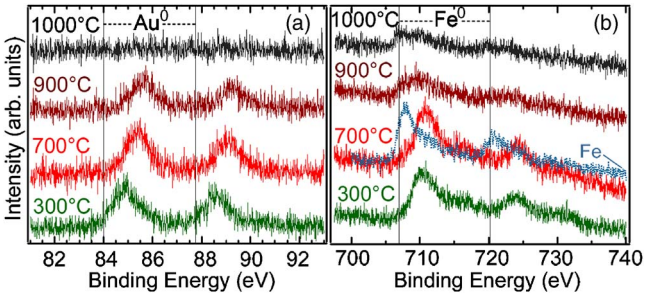

FIG. 2. (Color online) XPS spectra (Al $K\alpha$, 1486.6 eV) of the Au $4f$ (a) and Fe $2p$ (b) core levels of AuFe NPs supported on $TiO_2(110)$ measured after an O_2-plasma treatment and subsequent annealing in UHV from 300 to 1000 °C. Reference lines corresponding to bulk Au $4f$ and Fe $2p$ levels are also plotted. In (b), the spectrum labeled as Fe corresponds to monometallic Fe NPs deposited on TiO_2.

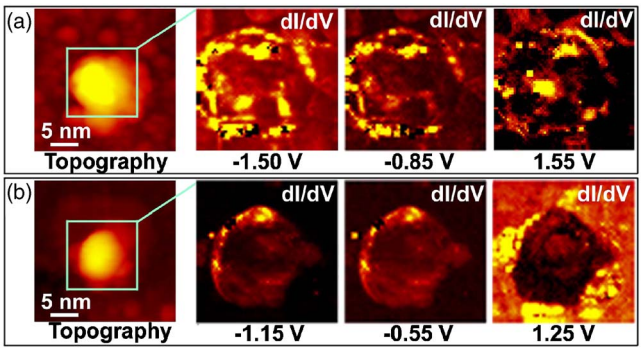

FIG. 3. (Color online) STM images (topography) and dI/dV maps of two typical AuFe NPs supported on $TiO_2(110)$ measured after O_2-plasma treatment and annealing at 300 °C (a) and 900 °C (b). dI/dV maps are recorded using a (64×64) grid over an area of 12.5×12.5 nm^2 (light blue squares).

NPs on $TiO_2(110)$ after O_2-plasma treatment and subsequent annealing at 300 °C (a), 900 °C (b), and 1000 °C [(c) and (d)]. Size-selected AuFe NPs with well-defined interparticle distances (l) can be observed. STM images from similarly synthesized Au NPs showing hexagonal NP arrangement over larger substrate areas can be found in Ref. 13. In the temperature range from 300 to 900 °C, a stable l of ~49 nm was measured. However, a significant change in the morphology of the $TiO_2(110)$ surface (i.e., a decrease in the roughness caused by the O_2 plasma) was observed after annealing at 900 °C [Fig. 1(b)]. At this temperature, the onset of the $TiO_2(110)$-(1×1) surface reconstruction appears. In addition, at least three TiO_2 atomic layers are removed in the vicinity of the AuFe NPs upon annealing at 900 °C. By contrast, the presence of the AuFe NPs seems to stabilize TiO_2 layers underneath and on the perimeter of the NPs. No diffusion of AuFe NPs or coarsening was observed at least up to 900 °C. This remarkable stability reflects the strong interaction between the AuFe NPs and the underlying TiO_2 support. Only a small decrease in the size of NPs was observed after annealing from 300 °C (height $h=4.6\pm0.4$ nm) to 800 °C (4.3 ± 0.3 nm). However, the annealing at 900 °C significantly reduced the average NP size to $h=3.2\pm0.3$ nm. This height change is likely to result from (i) atomic desorption from the cluster surface above 800 °C and (ii) a change in the NP shape (flatter NPs). After annealing at 1000 °C, the hexagonal NP arrangement is lost [Fig. 1(c)], bimodal size distribution ($h_1=2.5\pm0.5$ nm, $h_2=1.0\pm0.6$ nm) is observed. Further, large terraces of the $TiO_2(110)$-(1×1) reconstruction with atomic rows along the [001] direction appear[12] [Fig. 1(d)].

XPS data obtained after O_2 plasma and annealing at 300 °C indicate the presence of Fe^{3+} (710.5 eV, $2p_{3/2}$) in the AuFe NPs (Fig. 2). The large binding energy (BE) measured for Au (0.8 eV larger than bulk Au, 84.0 eV) is attributed to the interaction with the nearby Fe_2O_3 environment. At 700 °C, a further increase in the BE of Au is observed, indicating the formation of the AuFe alloy (85.4 eV, $4f_{7/2}$). However, no significant shift in the Fe $2p$ core level is observed, suggesting that the BE of Fe in a AuFe alloy (710.9 eV) is similar to that of Fe_2O_3. To corroborate this point, the BE of similarly synthesized monometallic Fe clusters was measured after annealing at 700 °C [curve "Fe" in Fig. 2(b)]. In this case, a much lower BE value was obtained (707.7 eV, $2p_{3/2}$). At 900 °C, a marked decrease in the Fe signal of the AuFe NPs is observed (~40%), while the Au signal is nearly constant (~3% decrease due to minimal Au desorption at this temperature). Since Au is expected to desorb at lower temperatures than Fe, the stronger reduction in the XPS Fe signal is most likely due to Au segregation to the NP surface. The complete desorption of Au and the partial Fe reduction (Fe^0, 707 eV) as well as desorption occur at 1000 °C. The oxidized Fe species observed at 1000 °C are attributed to the Fe/TiO_2 interface.

Spatially resolved STS measurements have been performed using I-V acquisition grids centered on individual AuFe NPs in order to get insight into the electronic local density of states, alloy composition, and segregation phenomena at the nanoscale.

Figure 3 shows dI/dV maps recorded on two AuFe NPs after annealing at 300 °C [Fig. 3(a)] and 900 °C [Fig. 3(b)]. An inhomogeneous dI/dV distribution is observed after the low-temperature annealing. Further, the presence of individual grains within each AuFe NP is evident from Fig. 3(a) at 1.55 V. Similar dI/dV distributions were observed on several other NPs in our sample after annealing at 300 °C, indicating the lack of alloying between Au and Fe. Annealing at 900 °C [Fig. 3(b)] results in a featureless dI/dV distribution within individual AuFe NPs, indicating the coalescence of the Au and Fe grains. A more in-depth study of the electronic properties of these NPs can be made by analyzing normalized dI/dV curves $[(dI/dV)/(I/V)\propto(\mathrm{LDOS})]$ obtained at specific NP locations.

Figure 4 shows normalized dI/dV curves recorded on isolated AuFe NPs after annealing at 300 °C (a), 700 °C (b), and 900 °C (c). Following Ref. 14, a moderate broadening factor, $\varepsilon^2=0.002$ $(\mathrm{nA/V})^2$, has been applied to the total conductivity $\overline{(I/V)}=\sqrt{(I/V)^2+\varepsilon^2}$ to eliminate excessive noise in the bandgap region and the divergence of $(dI/dV)/(I/V)$ at the band edges. The curves labeled "R-TiO_2" were recorded on the TiO_2 surface far away from AuFe NPs after each thermal treatment. In Fig. 4(a), the LDOS of the TiO_2 substrate exhibits a net bandgap of ~1 eV, with the edge of the conduction band minimum located ~0.3 eV above E_F. Within the bandgap region, the increase of the LDOS at ~−0.9 and ~−1.4 eV is due to the presence of O vacancies on the reduced TiO_2 surface (R-TiO_2) after annealing at 300 °C. The creation of O vacancies results in free electron charge which is partially transferred to adjacent Ti $3d$ levels. These levels are associated with Ti ions in the 3^+ oxidation state and appear as occupied states within the bandgap.[15] In Fig. 3(b), the LDOS of R-TiO_2 shows an enhancement of the

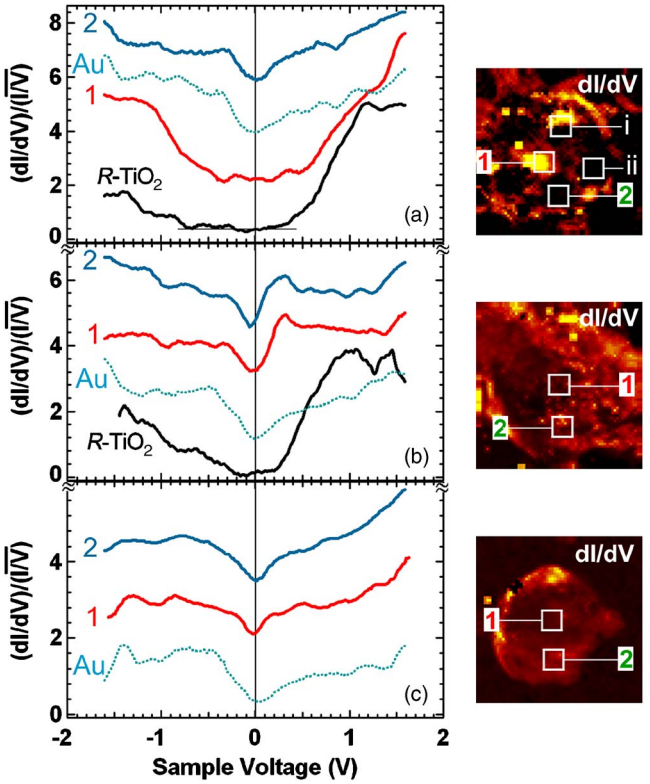

FIG. 4. (Color online) Normalized differential conductivity curves measured on three size-selected AuFe NPs deposited on $TiO_2(110)$ after O_2 plasma and subsequent annealing at 300 °C (a), 700 °C (b), and 900 °C (c). The insers are dI/dV images indicating the position of the acquisition grids used. Each curve was obtained from the average of 64 individual I-V curves taken over different 1.5×1.5 nm^2 regions inside each NP. Dotted curves were obtained on a reference sample containing pure Au NPs of similar size deposited on $TiO_2(110)$ and annealed in UHV at identical temperatures.

conductivity in the bandgap (at −0.6 and −1.1 eV) resulting from the increase of Ti 3d states as additional O vacancies are created after annealing at 700 °C. A similar effect is observed after annealing at 900 °C (not shown).

Curve 1 in Fig. 4(a) was acquired at the top of a AuFe NP after annealing at 300 °C. The large bandgap (~0.75 eV) measured at this NP location can be attributed to oxidized Fe atoms in Fe_2O_3, since no metal-to-nonmetal transition related to quantum size effects is expected for a NP of this size (h=4.6 nm). Our XPS measurements corroborate the presence of iron atoms in the Fe^{3+} state at this temperature [Fig. 2(b)] due to the O_2-plasma treatment used to remove the encapsulating polymeric shell. Curve 2 in Fig. 4(a), recorded in the perimeter area of this AuFe NP, does not show such a large bandgap and we identify this location as a gold-rich region. The Au_2O_3 formed upon NP exposure to O_2 plasma is easily decomposed well below 300 °C. A similar curve was measured on a pure Au NP (curve "Au") from a reference sample with Au NPs on $TiO_2(110)$ annealed at 300 °C. Curves comparable to 1 and 2 (not shown) were measured on regions (i) and (ii), respectively, in Fig. 4(a). From our STS analysis, we infer that Au and Fe at this temperature are phase separated.

After annealing at 700 °C [Fig. 4(b)], curves 1 and 2 show a peak in the LDOS ~0.25 eV above E_F which is attributed to Fe surface states. These states are not observed in the LDOS obtained on a pure Au NP after an identical thermal treatment (curve Au). Band structure calculations[11] of the bulk Fe(001) surface show the presence of states with high localization and surface amplitudes along the $\bar{\Gamma}$-$\bar{X}$ direction of the Brillouin zone. However, mainly states at the center of the Brillouin zone ($\bar{\Gamma}$) above E_F are accessible to STS, and they arise from nearly unperturbed $d_{3z^2-r^2}$ orbitals.[11] The observation of the $\bar{\Gamma}$ surface state at different locations within the AuFe NPs' surface indicates the formation of a Au–Fe alloy at 700 °C. Bischoff *et al.*[10] also reported the formation of an alloyed surface layer for the Au/Fe(001) system after annealing at 700 °C.

The composition of the NPs' surface was found to change after annealing at 900 °C, namely, the spectroscopic feature from Fe states vanishes from the LDOS [Fig. 4(c)] (curves 1 and 2). This indicates a decrease in the number of Fe atoms at the NP surface, leading to a Au-rich surface due to the segregation of Au atoms toward the NP surface. This is consistent with our XPS data at 900 °C [Fig. 2(b)]. The favorable segregation of Au atoms to the NP surface may result from the lower surface energy γ of Au (γ_{Au}=1.55 J/m^2) as compared to Fe (γ_{Fe}=3.47 J/m^2),[16] as well as from the larger atomic volume of Au (~12.5 Å^3) with respect to Fe (~8.0 Å^3).[17]

In conclusion, high stability was observed for $Au_{0.5}Fe_{0.5}$ NPs supported on $TiO_2(110)$ up to an annealing temperature of 900 °C. The preservation of the initial hexagonal NP arrangement indicates strong cluster-support interactions. STS measurements revealed that separated Au and Fe grains coexist within an individual AuFe NP after annealing at 300 °C. A homogenous alloy is formed upon annealing at 700 °C, with the marked appearance of an iron $d_{3z^2-r^2}$ surface state. Further annealing at 900 °C was found to induce the formation of a Au-rich NP surface due to gold segregation.

This work was supported by NSF (CAREER, No. 0448491) and ACS-PRF (42701-G5) awards.

[1] C. T. Campbell, Annu. Rev. Phys. Chem. **41**, 775 (1990).
[2] J. A. Rodriguez, Surf. Sci. Rep. **24**, 225 (1996).
[3] G. F. Wang, M. A. Van Hove, P. N. Ross, and M. I. Baskes, Prog. Surf. Sci. **79**, 28 (2005).
[4] A. Kolmakov and D. W. Goodman, Rev. Sci. Instrum. **74**, 2444 (2003).
[5] A. F. Carlsson, M. Naschitzki, M. Baumer, and H. J. Freund, J. Phys. Chem. B **107**, 778 (2003).
[6] A. M. Molenbroek, J. K. Norskov, and B. S. Clausen, J. Phys. Chem. B **105**, 5450 (2001).
[7] R. M. Finch, N. A. Hodge, G. J. Hutchings, A. Meagher, Q. A. Pankhurst, M. R. H. Siddiqui, F. E. Wagner, and R. Whyman, Phys. Chem. Chem. Phys. **1**, 485 (1999).
[8] M. F. Crommie, C. P. Lutz, and D. M. Eigler, Phys. Rev. B **48**, 2851 (1993).
[9] A. Davies, J. A. Stroscio, D. T. Pierce, and R. J. Celotta, Phys. Rev. Lett. **76**, 4175 (1996).
[10] M. M. J. Bischoff, T. K. Yamada, and H. van Kempen, Phys. Rev. B **67**, 165403 (2003).
[11] J. A. Stroscio, D. T. Pierce, A. Davies, R. J. Celotta, and M. Weinert, Phys. Rev. Lett. **75**, 2960 (1995).
[12] U. Diebold, J. Lehman, T. Mahmoud, M. Kuhn, G. Leonardelli, W. Hebenstreit, M. Schmid, and P. Varga, Surf. Sci. **411**, 137 (1998).
[13] A. Naitabdi, L. K. Ono, and B. Roldan-Cuenya, Appl. Phys. Lett. **89**, 043101 (2006).
[14] M. Prietsch, A. Samsavar, and R. Ludeke, Phys. Rev. B **43**, 11850 (1991).
[15] Z. Klusek, A. Bustakiewicz, and P. K. Datta, Surf. Sci. **600**, 1619 (2006).
[16] O. S. Hernan, A. L. V. de Parga, J. M. Gallego, and R. Miranda, Surf. Sci. **415**, 106 (1998).
[17] J. Tersoff, Phys. Rev. Lett. **74**, 434 (1995).